Neogene paleoelevation of intermontane basins in a narrow, compressional mountain range, southern Central Andes of Argentina

Gregory D. Hoke [a,*], Laura B. Giambiagi [b], Carmala N. Garzione [c], J. Brian Mahoney [d], Manfred R. Strecker [e]

[a] *Department of Earth Sciences, Syracuse University, Syracuse, NY 13244, USA*
[b] *Instituto Argentino de Glaciología Nivilogía y Ciencias Ambientales, CONICET, Mendoza, 5500, Argentina*
[c] *Department of Earth and Environmental Science, University of Rochester, Rochester, NY 14627, USA*
[d] *Department of Geology, University of Wisconsin Eau Claire, Eau Claire, WI 54702, USA*
[e] *Institute für Erd und Umweltwissenschaften, Universität Potsdam, 14476, Potsdam, Germany*

A B S T R A C T

The topographic growth of mountain ranges at convergent margins results from the complex interaction between the motion of lithospheric plates, crustal shortening, rock uplift and exhumation. Constraints on the timing and magnitude of elevation change gleaned from isotopic archives preserved in sedimentary sequences provide insight into how these processes interact over different timescales to create topography and potentially decipher the impact of topography on atmospheric circulation and superposed exhumation. This study uses stable isotope data from pedogenic carbonates collected from seven different stratigraphic sections spanning different tectonic and topographic positions in the range today, to examine the middle to late Miocene history of elevation change in the central Andes thrust belt, which is located immediately to the south of the Altiplano-Puna Plateau, the world's second largest orogenic plateau. Paleoelevations are calculated using previously published local isotope-elevation gradients observed in modern rainfall and carbonate-formation temperatures determined from clumped isotope studies in modern soils. Calculated Neogene basin paleoelevations are between 1 km and 1.9 km for basins that today are located between 1500 and 3400 m elevation. Considering the modern elevation and $\delta^{18}O$ values of precipitation at the sampling sites, three of the intermontane basins experienced surface uplift between the end of deposition during the late Miocene and present. The timing of elevation change cannot be linked to any documented episodes of large-magnitude crustal shortening. Paradoxically, the maximum inferred surface uplift in the core of the range is greatest where the crust is thinnest. The spatial pattern of surface uplift is best explained by eastward migration of a crustal root via ductile deformation in the lower crust and is not related to flat-slab subduction.

© 2014 Elsevier B.V. All rights reserved.

1. Introduction

Constraints on the elevation history of mountain ranges provide topographic boundary conditions that are important for evaluating tectonic (DeCelles et al., 2009; Hilley et al., 2004; Isacks, 1988; Jordan et al., 1983), geodynamic (Meade and Conrad, 2008; Whipple and Meade, 2006; Willett, 1999) and paleoclimate models (Jeffery et al., 2012). Over the past decade, large orogenic plateaus have been the major focus of paleoaltimetry studies (e.g., Garzione et al., 2000, 2008; Mix et al., 2011; Rowley and Currie, 2006) in an attempt to couple deformation histories and geody-

namic processes with elevation history (Ehlers and Poulsen, 2009; Hoke and Garzione, 2008; Lamb, 2011; Mulch et al., 2006). However, elongate, longitudinally oriented mountain ranges that are located at right angles or obliquely with respect to the prevailing wind directions and atmospheric moisture transport are especially attractive targets to assess the regional impact of topographic growth on atmospheric circulation patterns and ensuing changes in climate and surface processes. Yet, narrow, non-collisional mountain ranges dominated by fold-and-thrust belts, which should have simpler uplift and sedimentary histories, have received less attention (Blisniuk and Stern, 2005; Chamberlain et al., 1999; Hren et al., 2010). Measuring more than 7000 km in length and at the interception of two major precipitation regimes sourced in the southwest and northeast, respectively, the meridionally oriented
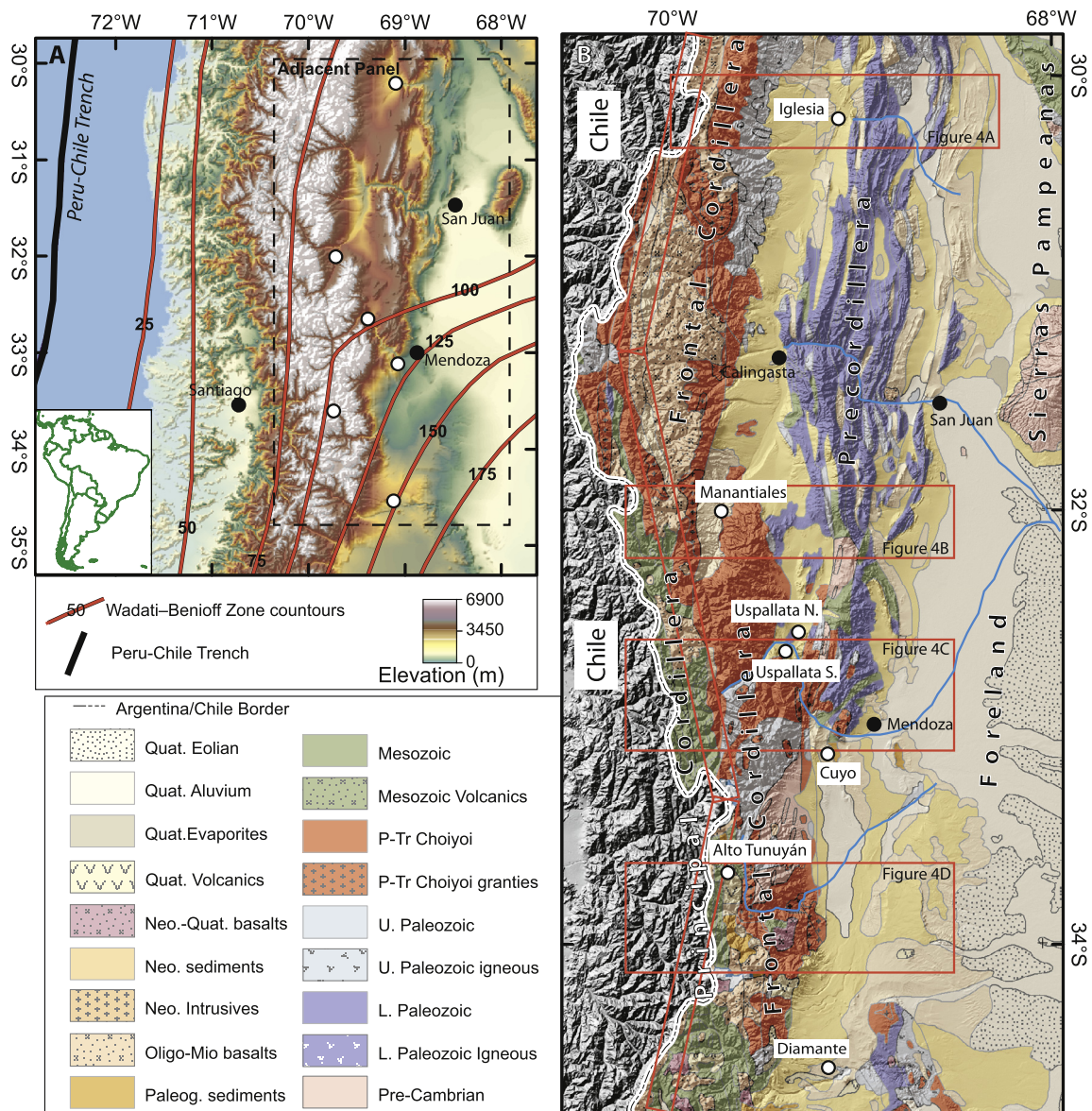
Fig. 1. Overview of the study area and sampling locations. A. Shaded relief topographic map generated from 250 m resolution SRTM data (http://srtm.csi.cgiar.org/). The contours of the subducting Nazca plate are from Cahill and Isacks (1992). Major cities are labeled with black dots for reference and the white dots are the locations of stratigraphic sections sampled in this study. The dashed line box indicates the outline of the area in B. B. Simplified geology of the study region from the 1:3,000,000 geologic map of Argentina showing the major geologic provinces, Cities (black circles) and the names and locations of the stratigraphic sections mentioned in the text (white circles).

Andes are a prime site to examine these relationships (Bookhagen and Strecker, 2008; Garreaud et al., 2009; Montgomery et al., 2001; Strecker et al., 2007).

Ideally, paleoaltimetry studies span sites likely to have remained at similar elevations through time as well as sites thought to have undergone significant elevation change over the same period. The eastern flanks of the southern central Andes in central Argentina between 30°S and 35°S (Fig. 1) contain a combination of largely synchronous late Cenozoic intermontane and foreland basin deposits rich in calcareous paleosols (Figs. 2A and 2B), making it an excellent locality for constraining elevation history in the context of crustal shortening (Fig. 2C). Furthermore, the magnitude of deformation at these latitudes is well-constrained (Allmendinger et al., 1990; Cristallini and Ramos, 2000; Giambiagi et al., 2012) with total shortening decreasing nearly threefold from north to south across the study area (Fig. 2C) and geophysical data indicating a 15 km decrease in crustal thickness over the same interval (Gans et al., 2011; Giambiagi et al., 2012). Despite these dramatic changes

in total crustal shortening and differences in geophysical characteristics, there is no significant change in mean elevation (Fig. 2D). This study uses the isotopic composition of pedogenic carbonates preserved in topographically distinct Miocene to Pliocene sedimentary basins to evaluate the spatial and temporal relationships between crustal thickening and topographic growth over a 500 km segment of the Andes with the goal of understanding what drives elevation change in narrow, linear mountain ranges.

2. Geologic and tectonic background

The western margin of the southern South American continent has been convergent since at least the Jurassic, if not earlier (Mpodozis and Ramos, 1989). An abrupt transition in the subduction angle of the Nazca Plate occurs at ∼33°S (Fig. 1), with the area to the north constituting the wider section of flat-slab subduction (Fig. 1; Anderson et al., 2007; Cahill and Isacks, 1992). South of 33°S, dip of the subducting slab returns to ∼30°
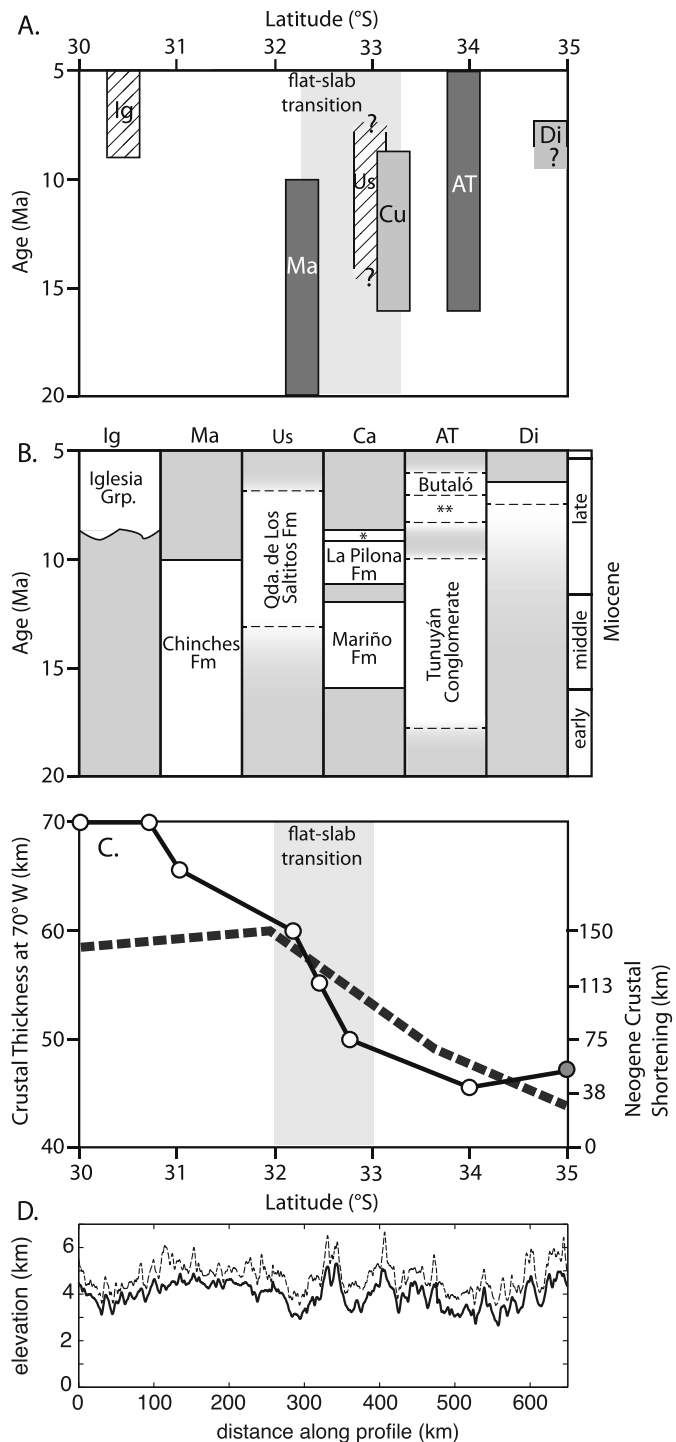
Fig. 2. A. Plot of the age range of sedimentary deposits versus latitude for the isotope data reported in the study; Di = Diamante Region; AT = Alto Tunuyán Basin; Ca = Cacheuta Basin; Us = Uspallata Basin; Ma = Manantiales Basin; and Ig = Iglesia Basin. B. Formation names of stratigraphic units and their age ranges, basin codes are the same as in A. The ∗ symbol refers to the Tobas Angosturas and Río de los Pozos formations (Irigoyen et al., 2000) and "∗∗" refers to the Palomares Formation (Giambiagi, 1999). C. Variations in crustal thickness and total Neogene crustal shortening with latitude. The left axis and solid line with dots represent crustal thickness determined from receiver functions from Gans et al. (2011) (white circles) and gravity data from Giambiagi et al. (2012) (gray circle). The right axis and dashed line are total crustal shortening with latitude (dashed line) compiled from Giambiagi et al. (2012), Allmendinger et al. (1990) and Cristallini and Ramos (2000). D. Swath topographic profile (15 km wide along) of average (solid) and maximum topography (dashed) along the range crest from 30°S to 35°S. Note that despite a dramatic drop in crustal shortening range elevations remain high south of 32°S.

(Cahill and Isacks, 1992). The initiation of flat-slab subduction is often invoked as the driving force behind all post-10 Ma crustal shortening north of 33°S, and is inferred by poorly constrained eastward migration of deformation and range uplift (e.g., Ramos et al., 2002). An important consequence of flat-slab subduction is the cessation of arc magmatism between 33°S and 27°S at ∼10–12 Ma (Kay et al., 1987; Kay and Mpodozis, 2002). The first active volcano south of the flat slab, Tupungatito volcano, is located at 33.3°S (Fig. 1A).

The physiographic and tectonic divisions of the eastern flanks of the Andes comprise the following morpho-tectonic provinces; from west to east, the Principal Cordillera, the Frontal Cordillera, the Uspallata–Calingasta–Iglesia wedge-top basin, the Precordillera, and the Sierras Pampeanas in the broken foreland (Fig. 1). The Principal Cordillera comprises the core of the orogen at these latitudes and consists of Mesozoic and Cenozoic sediments and volcanic rocks (Cristallini and Ramos, 2000; Farías et al., 2008; Giambiagi et al., 2003; Vicente, 2005). To the east, the Frontal Cordillera is dominated by the Permo-Triassic Choiyoi Group granites and rhyolites. The Paleozoic Precordillera terrane (Thomas and Astini, 1996) is a multiply deformed (Giambiagi et al., 2011) passive-margin sequence whose topographic expression ends at ∼33°S (Fig. 1). South of 33°S, the Frontal Cordillera comprises the steep topographic mountain front (Fig. 1), with the area to the east containing smaller localized uplifts that deform Neogene strata and are likely related to the Cenozoic inversion of extensional structures in the Mesozoic basement (García and Casa, 2014). Total Cenozoic shortening varies considerably from north to south between 30°S and 35°S. At 30°S late Cenozoic crustal shortening is ∼140 km (Allmendinger et al., 1990) and increases slightly at 32°S to ∼150 km (Cristallini and Ramos, 2000; von Gosen, 1992). Total shortening is dominated by thin-skinned deformation in the Precordillera and Principal Cordillera fold-and-thrust belts with thick-skinned behavior in the Frontal Cordillera. Towards the south shortening rapidly declines to ∼50 km (Giambiagi et al., 2012; Giambiagi et al., 2003) and is chiefly thick-skinned in style (Fig. 2C).

Cenozoic Andean mountain building began approximately between 25 and 18 Ma in the Principal Cordillera and possibly the Frontal Cordillera (Giambiagi et al., 2003; Hoke et al., 2014a; Jordan et al., 1996; Ramos et al., 2002), and is recorded in Miocene intermontane and foreland sedimentary basin sequences between 30°S and 35°S. Based on existing chronologic constraints, the onset of deformation in the Precordillera is diachronous from north to south. The initiation of deformation and sedimentation in the Precordillera began in the early Miocene at 30°S (Jordan et al., 1993), while surface uplift of the southernmost Precordillera, at ∼32.5°S, began at ∼10 Ma (Walcek and Hoke, 2012). A simple, continuous foreland basin with no preexisting topography in the Frontal Cordillera and Precordillera (e.g., Giambiagi et al., 2003; Ramos et al., 2002) and constant eastward migration of deformation towards the foreland has always been assumed as the initial starting condition of topographic evolution in this area. However, recent studies suggest significant pre-Neogene paleotopography in both the Frontal and Pre-cordilleras (Hoke et al., 2014a; Walcek and Hoke, 2012). Taken together, this suggests the existence of a broken foreland with compartmentalized, yet fluvially connected sedimentary basins during the Miocene.

This study focuses on sediments of the Manantiales (Jordan et al., 1996; Mirré, 1966), Alto Tunuyan (Giambiagi, 1999; Giambiagi et al., 2003) Uspallata (Cortés, 1993) and Iglesia (Beer et al., 1990; Ruskin and Jordan, 2007) intermontane basins along with the Cacheuta (Irigoyen et al., 2000) and Río Diamante foreland basins (Sruoga et al., 2005) (Figs. 2A and 2B). The Cacheuta and Manantiales basins were previously studied by magnetostratigraphy (Irigoyen et al., 2000; Jordan et al., 1996) and thus excellent

temporal control exists. The Alto Tunuyán Basin was described in detail by Giambiagi et al. (2001); the age of its sedimentary deposits is bracketed by volcanic strata and lithostratigraphic correlation. Prior to this study, three mapping units had been described in the Uspallata Basin (Cortés, 1993), and the sediments in the Río Diamante area of the Cacheuta Basin were described as part of 1:250,000 scale geologic mapping by the Argentine Geologic Survey (Sruoga et al., 2005). With our new data we provide detailed stratigraphic information for the Uspallata and Diamante Basins (see Supplementary material).

3. Methods

3.1. Sampling

We collected pedogenic and other authigenic carbonates exposed in intermontane and foreland basin successions on the eastern flanks of the Andes (Fig. 3). The stable isotope composition of authigenic carbonate formed in soils records information about the types or productivity of vegetation, the isotopic composition of meteoric waters at the time the soil formed (e.g., Cerling and Quade, 1993), and may be used to reconstruct past elevations (e.g., Rowley and Garzione, 2007). Pedogenic carbonate samples were collected at depths >30 cm below the contact with overlying beds to avoid unintentionally sampling the upper 40 cm of the original soil profile, as studies of modern soils (e.g. Cerling and Quade, 1993) clearly demonstrate that $\delta^{18}O$ and $\delta^{13}O$ are influenced by the air/soil interface. We measured three stratigraphic sections (Uspallata N, S and Río Diamante; see Supplementary material) in addition to the localities with previous detailed stratigraphic descriptions. In some cases, preexisting data were augmented with additional field observations and the collection of samples for geochronology. Pedogenic carbonate samples were not collected from areas with secondary calcite (veins, etc.). Thin sections of a subset of samples were examined for textural evidence of recrystalization and secondary precipitation (Fig. 3C and supplementary Fig. 1).

3.2. Stable isotope analysis

All carbonate samples were processed and analyzed for $\delta^{18}O$ and $\delta^{13}C$ values in the University of Rochester's Stable Isotope Laboratory on a Thermo DeltaPLUS XL CF-IRMS using a GasBench II peripheral device. Samples were visually inspected under a binocular microscope to ensure removal of any secondary calcite before pieces were and homogenized into a powder using a mortal and pestle. Samples were treated with 30% hydrogen peroxide for 20 min to remove organic matter and then dried, weighed and placed in vials. Vials were filled with He carrier gas and reacted with phosphoric acid at 60 °C for a minimum of two hours. Analytical precision (1σ) for individual analyses of a sample is 0.06‰ and 0.12‰ for $\delta^{13}C$ and $\delta^{18}O$, respectively. All δ values are reported relative to VPDB (see Supplementary materials).

3.3. Geochronology

To provide better age constraints for our stratigraphic section we radiometrically dated zircons from two samples using either ID-TIMS or LA-ICP-MS. Zircons were separated from a pumaceous tuff in the Río Diamante section (DIA-07-23) and a sandstone in the Uspallata area (04JBM08) using standard techniques of rock crushing, disc milling, water table concentration and heavy liquid separation. Zircons for DIA-07-03 were hand-picked with a binocular microscope under cross polarized light. Detrital zircons from 04JBM08 were selected at random by dumping a pure zircon mineral separate onto a grain mount. Six zircons from sample

Fig. 3. A. Photo of synorogenic sediments in the Uspallata Basin with prominent paleosol horizon (pink area) in the center of the photo with 45 cm long rock pick for scale. Dashed lines indicate areas of carbonate nodules weathering out of the outcrop. B. Close up of boxed area in A detailing the pedogenic carbonates weathering out of the rock exposure. C. Photomicrograph of a typical pedogenic carbonate nodule from sample (GH-06-15c). (For interpretation of the references to color in this figure legend, the reader is referred to the web version of this article.)

DIA-07-23 were analyzed by ID-TIMS at Boise State University (see supplementary data) and 04JBM08 was analyzed at the University of Arizona Laserchron Center (Gehrels et al., 2008).

3.4. Paleoelevation estimates

Reconstructing past elevations using pedogenic carbonates requires empirical (e.g. Poage and Chamberlain, 2001) and/or theo-

retical constraints (Rowley, 2007) on modern and, if possible, past isotope-elevation gradients. Similarly, constraints on the temperature of carbonate formation are important for accurate elevation estimates of $\delta^{18}O$ because isotopic fractionation of oxygen is temperature dependent.

We estimate paleoelevations using the isotope-elevation gradients determined from published weighted mean $\delta^{18}O$ of precipitation (Hoke et al., 2013). A -1‰ shift in $\delta^{18}O$ is also applied to the isotope-elevation relationship to account for a largely ice-free northern hemisphere during the Miocene. $\delta^{18}O$ VPDB values from carbonates are converted to $\delta^{18}O$ VSMOW based on the empirical temperature dependent fractionation factor given in Kim and O'Neil (1997). Clumped isotope (Eiler, 2007) temperature determinations from a study in the Mendoza River Valley (Peters et al., 2013), demonstrate that the temperatures of pedogenic carbonate formation in present-day soils are insensitive to elevation yielding mean temperatures of ~20 °C for elevations between 1.1 and 2.4 km; we therefore use a value of 20 ± 2.5 °C to convert from $\delta^{18}O$ VPDB to $\delta^{18}O$ VSMOW. An elevation and its uncertainty is calculated for each reported pedogenic carbonate $\delta^{18}O$ value at a sampling locality by a Monte Carlo simulation using 1000 randomly selected variations in the input parameters based on their respective uncertainties. The mean and standard deviation of each individual Monte Carlo simulation is then used to determine the uncertainty weighted mean elevation and uncertainty for each site following that of Hoke et al. (2014b).

4. Results

4.1. Thin sections

A total of 13 thin sections from the Cacheuta Basin were examined for evidence of recrystallization or strong diagenetic overprinting; 12 show primary micritic textures (supplementary Fig. 1b) with very minor spary calcite occasionally filling dessication cracks (Supplementary material Fig. 3c). One thin section, from a calcrete horizon at the base of the Mariño Formation, shows the primary texture of radial crystals around rhizoliths (supplementary Fig. 1b; Klappa, 1980).

4.2. Geochronology

The analysis of 6 zircons from the Río Diamante section sample DIA-07-23 yields a U–Pb age of 6.753 ± 0.011 Ma (see supplementary data). The youngest age in detrital zircon ages from sample 04JBM08, from the lowest part of the exposed stratigraphy in the Uspallata Basin, yield 3 overlapping LA-ICMPS zircons with a weighted mean age of 11.7 ± 0.8 Ma (see supplementary data).

4.3. Stable Isotopes of O and C

We report the stable isotopic composition of 414 pedogenic carbonate samples measured from five sedimentary basins (supplementary data Table 1). Average sampling density varies between 8 m per sample in the southern Uspallata section to 38 m per sample in the Manantiales Basin.

4.3.1. Manantiales Basin

The 78 samples from the >3000 m thick Manantiales Basin sequence (Fig. 1; Jordan et al., 1996) have $\delta^{13}C$ values between -7.4‰ and -1.4‰ VPDB (Fig. 4A) with a mean of -4.4‰ ± 1.3. Despite the 6‰ spread in $\delta^{13}C$ values in the part of the section that corresponds to the interval between 19 and 12 Ma, mean $\delta^{13}C$ values are ~5‰. A pronounced shift towards more positive $\delta^{13}C$ values occurs between 12 and 10 Ma (Fig. 4A). $\delta^{18}O$ values are between -14.9‰ and -8.0‰ VPDB with an average value and standard deviation of -11.5‰ ± 1.5 (Fig. 4A).

4.3.2. Alto Tunuyán Basin

The 1300 m thick section in the Alto Tunuyán Basin (Fig. 1) spans three formations (Giambiagi, 1999; Fig. 2B), two of which yielded pedogenic carbonate. $\delta^{13}C$ values for the paleosol bearing, middle Miocene Tunuyán Conglomerate (59 samples) range between -4.8‰ and -0.2‰ VPDB, with a mean value of -2.3‰ ± 1.2 (Fig. 4B). Similarly, $\delta^{18}O$ values span -10.9‰ to -5.4‰ VPDB with a mean value of -7.8‰ ± 1.3 (Fig. 4B). The 200 m thick upper Miocene Bútalo Formation (23 samples) exhibits variability similar to that observed in the underlying Tunuyán Conglomerate with $\delta^{13}C$ and $\delta^{18}O$ values between -10.3‰ to -5.9‰ and -6‰ to 0‰, respectively (Fig. 4B). Mean values for $\delta^{13}C$ and for $\delta^{18}O$ are -2.0 ± 1.5 and -8.1 ± 1.3, respectively.

4.3.3. Cacheuta Basin

Samples from the 16-9 Ma Cacheuta Basin (Fig. 1) were collected from four of Irigoyen et al.'s (2000) dated sections spanning the Mariño, La Pilona, Tobas Angosturas and Río de los Pozos Formations, and thus provide significant temporal overlap and geographic distribution. We separate the middle Miocene Mariño Fm (51 samples) and late Miocene La Pilona and Río de los Pozos Formations (64 samples). Middle Miocene $\delta^{13}C$ values are between -7.6‰ and -2.8‰ with a mean of -5.1‰ ± 1.0, while $\delta^{18}O$ values are from -10.6‰ to -2.7‰ and average -8.8‰ ± 1.5 (Fig. 4E). Late Miocene samples range in $\delta^{13}C$ and $\delta^{18}O$ from -7.3‰ to -3.1‰ (mean = -5.5‰ ± 1.0) and -9.5‰ to -5.00‰ (mean of -7.3‰ ± 1.0), respectively (Fig. 4E).

4.3.4. Río Diamante section

The late Miocene Rio Diamante section (Fig. 1) is 160 m thick and yielded 14 pedogenic carbonate samples. $\delta^{13}C$ and for $\delta^{18}O$ values range from -7.6‰ to -2.8‰ (mean of -5.1‰ ± 1.73) and -9.8‰ to -5.9‰ (mean of -7.8‰ ± 1.1), respectively (Fig. 4F).

4.3.5. Uspallata Basin

Based on the availability of geochronologic constraints, sedimentary rocks of the Uspallata Basin (Fig. 1) are divided into two separate sections north and south of the Río Mendoza. Samples from the section north of the river (75 samples) have $\delta^{13}C$ values between -9.13‰ and -1.86‰ (mean value of -6.8‰ ± 1.2; Fig. 4C). $\delta^{18}O$ values are between -10.7‰ and -5.1‰ (mean value of 7.2‰ ± 1.0; Fig. 4C). South of the river (50 samples), the average pedogenic carbonate $\delta^{13}C$ is -3.1‰ ± 0.8, with a range of -5.4‰ to -2.2‰ (Fig. 4D). $\delta^{18}O$ values have an average of -11.2‰ ± 1.2 and vary between -14.3‰ to -9.3‰ (Fig. 4D).

4.4. Calculated soil water isotopes and paleoelevations

Soil water isotopic compositions and paleoelevations are calculated for each of the basins and, in some cases, elevations were calculated for individual formations within a basin (Fig. 5; Table 1). Along with our new data, we also calculated elevations and soil water isotopic compositions on a subset of the stable isotope data reported for the Iglesia Basin (Ruskin and Jordan, 2007; Fig. 1). Calculated elevations range from 1100 m to 1900 m (Table 1) and are compared to swath profiles of the present-day topography (Fig. 5) as well as to the mean basin elevations where the samples were collected (Fig. 6).

5. Discussion

Here, we present Miocene stable isotope data between 35°S and 32°S. Given this large latitudinal range, our data have the potential to elucidate topographic and paleoenvironmental change within an important transition in the major atmospheric circulation
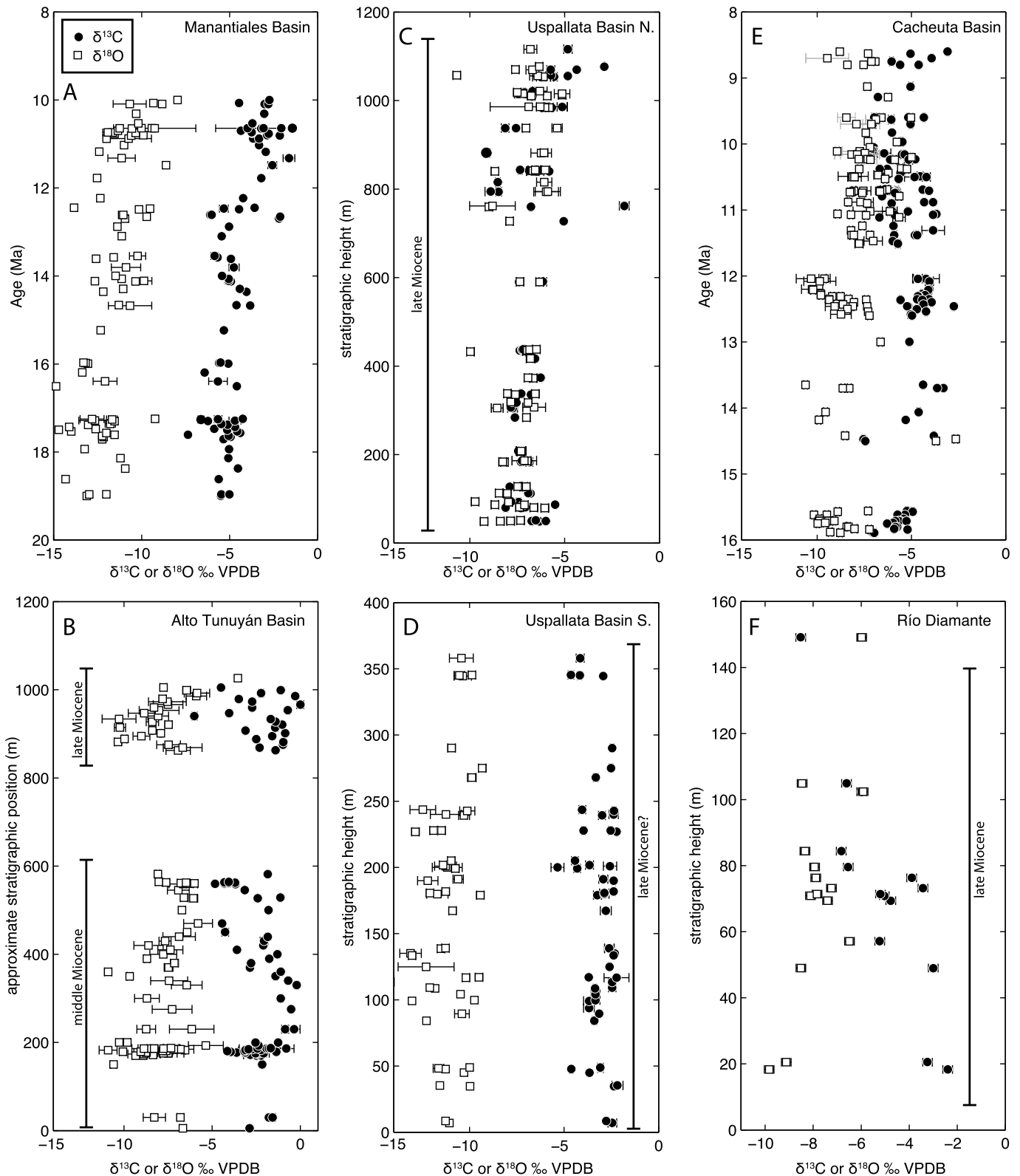
Fig. 4. Stable isotope data from the six stratigraphic sections sampled in this study. The *Y* axis is given as either stratigraphic height or time in Ma, depending on whether a magnetostratigraphic age model exists for the section. Error bars represent the uncertainty on the mean of multiple analyses.

systems impacting the southern hemisphere (e.g., Haselton et al., 2002). Our strategy of sampling pedogenic carbonates from a variety of elevations and tectonic positions, as well as from sections reflecting different episodes and styles of mountain building in the southern Central Andes between 30°S and 35°S, provides a

strong context for evaluating the topographic evolution of the orogen and its relationship with the timing of crustal thickening and lateral expansion of a growing crustal root. With our dataset we are able to monitor variability in stable isotope compositions of consistently low-elevation sites east of the topographic range front

(i.e., Cacheuta and Río Diamante) in order to identify regional paleoenvironmental shifts that could confound any paleoelevation estimates. Here, we treat $\delta^{13}C$ values as indicators of changes in paleoecology (e.g., Cerling and Quade, 1993), while $\delta^{18}O$ values reflect the isotopic composition of soil water, which we assume to be little modified from its original meteoric source (Hoke et al., 2013).

The $\delta^{13}C$ value of pedogenic carbonates reflects both the isotopic composition of vegetation (e.g. C_3 and C_4 plants) growing at the surface and the soil respiration rate (soil CO_2 produced by roots) (Cerling and Quade, 1993). Expansion of C_4 plants in NW Argentina is documented to have occurred at ~7 Ma based on pedogenic carbonates data (Latorre et al., 1997), and possibly as early

as 9 Ma based on rodent tooth enamel (Hynek et al., 2012). Consequently, much of our isotopic record predates the expansion of C_4 plants. Thus we expect a dominance of C_3 vegetation and interpret $\delta^{13}C$ values to reflect soil productivity instead of changes in the mixture of C_3 and C_4 vegetation. Our $\delta^{13}C$ values are consistent with values measured in low-vegetation density Holocene soils (Hoke et al., 2009; Peters et al., 2013) between 1.1 and 3.2 km elevation. The overall low variability and lack of long-term shifts in our $\delta^{13}C$ data from all sites (Fig. 4) implies relatively stable climate conditions during the middle to late Miocene. We interpret this to
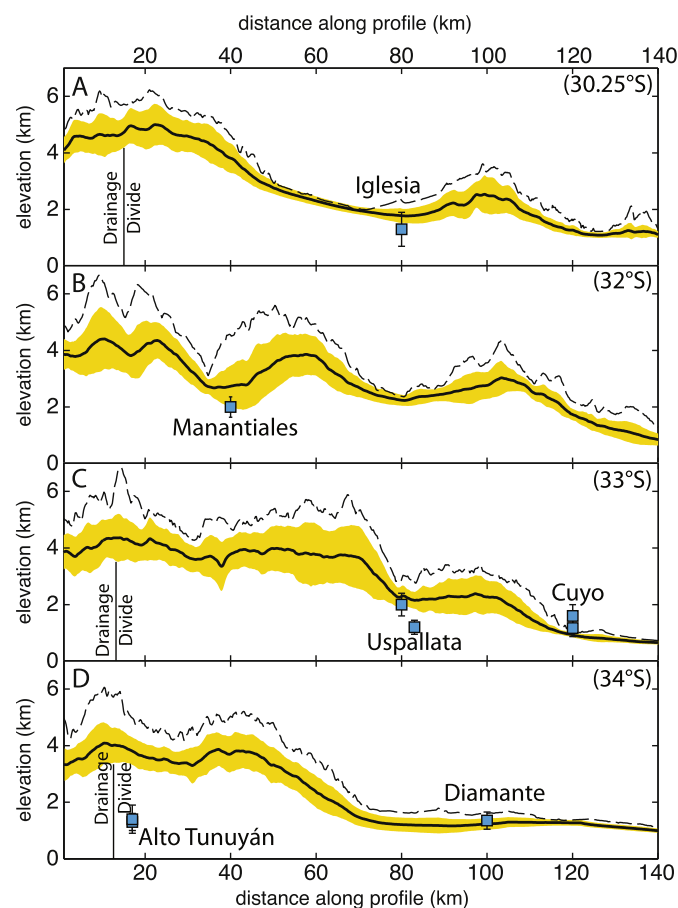

Fig. 5. Calculated middle to late Miocene paleoelevations and their 2-sigma uncertainties plotted with swath profiles of the modern topography and the 1-sigma deviation from the mean topography calculated in each swath. The location of each swaths A–D are shown in Fig. 1B.
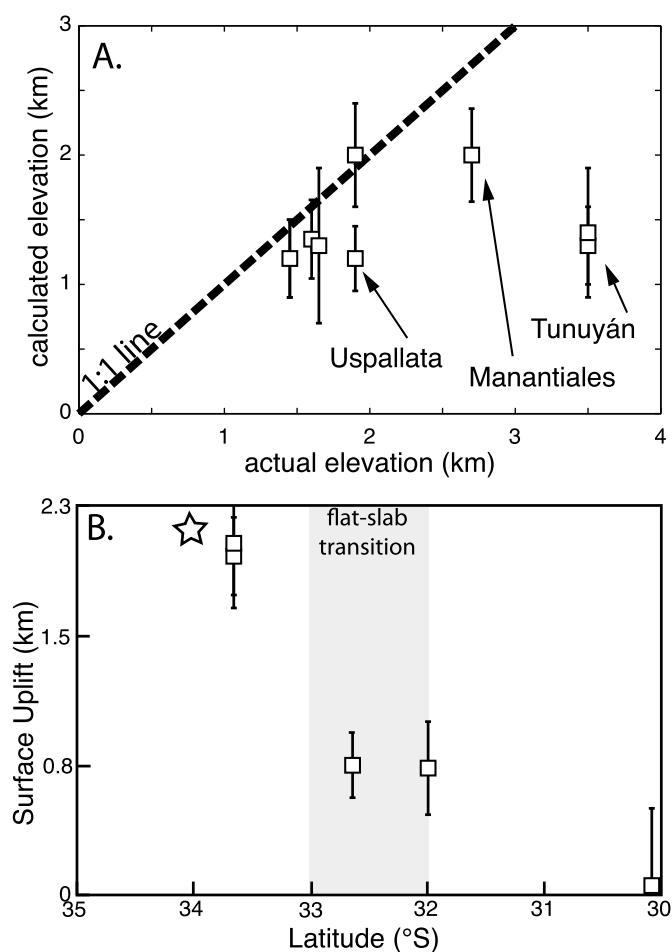

Fig. 6. A. Calculated elevations versus modern basin average elevation. B. Total latest Miocene to present surface uplift of intermontane basins versus latitude. Surface uplift is calculated by subtracting the modern elevation from the calculated paleoelevation. Star is between the two surface uplift amounts estimated by Farías et al. (2008).

Table 1
Calculated isotopic values and elevations.

Basin/Formation	Age	Modern elevation	$\delta^{18}O$ of soil water[b] (VSMOW)	Uncertainty (2σ)	Calculated elevation (m)	Uncertainty (2σ)	Number of samples
Iglesia[a]	9. to 4.6 (Ma)	1700	−6.7	0.8	1300	350	76
Manantiales	19 to 10 (Ma)	2700	−10	0.5	1900	400	78
Uspallata (N)	middle Miocene	1900	−5.9	0.5	1100	300	75
Uspallata (S)	late Miocene	1900	−10	0.5	1900	450	50
Cuyo/La Pilona	12 to 9 Ma	1650	−6	0.5	1200	350	64
Cuyo/Mariño	16 to 12 Ma	1650	−7.7	0.5	1500	400	51
Alto Tunuyán/Bútalo	late Miocene	3500	−6.8	0.8	1300	550	23
Alto Tunuyán/Cgl. Tunuyán	middle Miocene	3500	−6.7	0.5	1200	350	60
Diamante	late Miocene	1600	−6.5	1.0	1200	700	14

[a] Isotope data from Ruskin and Jordan (2007).
[b] Calculated from Kim and O'Neil (1997) assuming a temperature of $20 \pm 2.5\,°C$.

reflect the persistence of a semi-arid regional climate in the transition zone between the southern hemisphere westerly and easterly winds.

5.1. Low elevation sites

The lowest elevation basins at or near the boundary between the foreland and the eastern deformation front of the Andean fold-and-thrust belts form the baseline for how we estimate elevations in the intermontane basins to the west. The δ^{13}C isotopic records from the low-elevation Cacheuta Basin sites (Fig. 2; Figs. 4E and 4F) exhibit no significant shifts through time, which we interpret to record stable vegetation cover. Despite stable δ^{13}C values, a noticeable shift of 1.5‰ in δ^{18}O occurs near the boundary between the late Miocene La Pilona and middle Miocene Mariño Formations (Fig. 4E) in the Cacheuta Basin. However, this change is not large enough to lie outside the 1σ uncertainty of average values. Calculated paleoelevations ($\sim$1200 to 1600 m) match the modern topography within 2σ uncertainties (Table 1; Fig. 5 and Fig. 6). The $\sim$ 7 Ma Río Diamante section, shows a progressive decrease in δ^{13}C from an initial value of -2‰ to -7.6‰, which we interpret to reflect increased soil productivity in a C$_4$ environment. δ^{18}O values are less variable and the calculated paleoelevation of 1.2 km $\pm$ 0.7 km is within uncertainty of the modern basin elevation of 1.6 km.

Paleoelevations determined from Neogene pedogenic carbonates east of the main Andean topographic front (Rio Diamante and Cacheuta Basin) are similar to those of present-day. However, these areas are $\sim$1 km higher than the $\sim$0.5 km elevations of the modern foreland east of the present-day deformation front (Fig. 1B). This can be viewed in two different ways: 1) sediments were deposited at or near their present elevation and thus demonstrate a high degree of confidence in our ability to accurately determine paleoelevations of sedimentary basins; or 2) all carbonate has been isotopically altered during burial and diagenesis (e.g., Leier et al., 2009). Thin sections (Fig. 3C and supplementary Fig. 1) show micritic or rhizolith textures; thus, we rule out diagenetic alteration. Furthermore, based on the modern climate system, the isotopic composition of Atlantic-sourced rainfall does not vary significantly until it reaches the lower elevation sectors of the Andes (Insel et al., 2013; Jeffery et al., 2012; Sturm et al., 2007), which is locally at $\sim$850 m (Hoke et al., 2009); thus, modeled elevations are insensitive below $\sim$850 m or ~-5‰ VSMOW (Hoke et al., 2009, 2013). Therefore, we argue that our calculated low paleoelevations for basins east of the range front are accurate, and suggest that these areas have been at or near their present elevations since the middle and late Miocene.

5.2. Wedge-top basins

The Uspallata and Iglesia basins are the northern and southern extremes of a 350 km-long wedge-top basin between the Frontal Cordillera and Precordillera thrust belts. A detailed study of latest Miocene to earliest Pliocene (9 to 4.5 Ma) paleosols of the Iglesia Basin led Ruskin and Jordan (2007) to conclude that they developed under generally semi-arid conditions with the potential appearance of C$_4$ plants at 6.9 Ma. They did not, however, examine their oxygen isotope data in the context of paleoelevation. We filtered their original dataset to remove samples with evidence of evaporative enrichment based on the positive co-variance between δ^{13}C and δ^{18}O (e.g., Rowley and Garzione, 2007), and calculated a late Miocene elevation of 1.4 km $\pm$ 0.3 km, which suggests the Iglesia basin had attained its present elevation before 9 Ma, consistent with the early Miocene onset of deformation of the western Precordillera (Jordan et al., 1993; Jordan et al., 2001).

The late Miocene sediments of the Uspallata Basin (Fig. 2) north of the Río Mendoza have average δ^{13}C and δ^{18}O values remarkably similar to that of the Iglesia Basin (Fig. 4D and C). Given the 2.5° of latitude between these sites, we suggest similar environmental conditions, reflecting soils with relatively high respiration rates dominated by C$_3$ vegetation. Walcek and Hoke (2012) determined the onset of deformation in the southern Precordillera to be $\sim$10 Ma, and total surface uplift to be 1.3 km. However, their approach did not determine when major surface uplift of the Precordillera occurred. The paleoelevation calculated for the northern section part of the Uspallata Basin (1.1 km $\pm$ 0.3 km), is consistent with the Iglesia Basin to the north, but 0.8 km lower than the modern elevation at Uspallata. The age of the basal part of the exposed synorogenic sediments at Uspallata are age equivalent with the La Pilona Formation if we take the youngest zircon ages of 12 Ma from the base of the exposed sediments in the Uspallata section to reflect their approximate age of deposition. Based on the inference of $\sim$12 Ma, we also assume the interval of gray tuffaceous sandstones $\sim$500 m up section to represent the equivalent of the Tobas Angosturas Formation, which directly overlies the La Pilona Formation (Irigoyen et al., 2000) and extends the age of the youngest sediments in this section to at least 8.5 Ma. We can therefore interpret the low elevations recorded by the pedogenic carbonates of the Uspallata Basin to represent deposition prior to the $\sim$10 Ma deformation and uplift of the southern Precordillera (Walcek and Hoke, 2012). No age constraints exist for the 400 m-thick stratigraphic section measured south of the Río Mendoza. However, the isotopic data from this area are in sharp contrast to those on the north side of the river, separated by only 10 km. Average δ^{13}C values increase by 4‰, and δ^{18}O values decrease by 4‰ relative to those north of the Río Mendoza. This suggests a major decrease in soil productivity, which might be expected with increasing elevation and associated increasing aridity. The elevation calculated from the δ^{18}O values is 1.9 km $\pm$ 0.5 km, identical to the modern basin elevation. We interpret this change in elevation to reflect rock uplift of the southern Precordillera; however, without chronologic constraints, this remains speculative. Alternative explanations for the observed shift in isotope compositions present more complicated scenarios. The southern Uspallata measured section is along nearly vertically dipping beds exposed against the fault contact between the Frontal Cordillera and the southern edge of the Uspallata Basin, thus it is possible that fluid flow focused near the fault could have diagenetically altered the δ^{18}O signal. However, we did not observe secondary vein calcite in the field and there are no faults cutting the measured section. It is also possible that the observed shift marks a significant change in climate or the source of precipitation (E or W sourced); however, any change in precipitation source would likely be tied to the construction of orographic barriers, which is what we posit.

5.3. Orogen interior basins

Giambiagi et al. (2001, 2003) presented the Alto Tunuyán Basin (Fig. 2) in the context of a classic foreland basin system (DeCelles and Giles, 1996), with deposition of the Tunuyán Conglomerate in the proximal foredeep, which was later dissected by the rising frontal Cordillera to the east (Palomares Fm). Later, the fine-grained Bútalo Formation was interpreted to represent ponding behind the topographic barrier of the Frontal Cordillera. As part of this model, it would be reasonable to assume that crustal shortening leading to the emergence of the Frontal Cordillera would have transitioned the Alto Tunuyán basin to a wedge-top environment and increased its elevation via surface uplift. However, calculated paleoelevations for the Tunuyán Conglomerate and the Bútalo Formation are 1.2 $\pm$ 0.4 km and 1.3 $\pm$ 0.6 km, respectively. Thus, during deposition of both formations, the basin was at elevations

similar to those now east of the Andean topographic front (see above). Furthermore, our elevation estimates point to 2 km of post-Bútalo, i.e. Pliocene to present-day, surface uplift in this area (Fig. 6). The magnitude and timing of surface uplift is consistent with surface uplift estimates on the western flanks of the range based on thermochronology, geochronology and tectonic geomorphology (Farías et al., 2008). Latest Miocene to present-day uplift of the Frontal Cordillera would imply rock uplift rates for the frontal Cordillera of at least 300 m/My.

The Manantiales Basin is situated west of the Uspallata–Calingasta–Iglesia trough on the western edge of the Frontal Cordillera in the headwaters of the Río de los Patos. How the Manantiales Basin is related to the Calingasta Valley and the larger Bermejo foreland is unclear due to a lack of exposure of basin sediments in the Calingasta Valley (Jordan et al., 1996). However, the >3 km accumulation of Miocene sediments (Fig. 2B) and their facies patterns (Jordan et al., 1996) suggests it behaved like a proximal foreland basin to the fold-and-thrust belts located to the west (Cristallini and Ramos, 2000). Our carbonate samples are from the same stratigraphic sections of the paleomagnetic reversal stratigraphy of Jordan et al. (1996), which spans elevations of 2.1 to 3.3 km. $\delta^{18}O$ and $\delta^{13}C$ values vary little throughout the 9 Ma record preserved in the Manantiales Basin strata (Fig. 4A), which suggests relatively stable conditions. Elevations calculated from the $\delta^{18}O$ values yield an estimate of 1.9 km $\pm$ 0.40 km, similar to that of the modern Río de los Patos Valley. This implies a modest amount of surface uplift of the Manantiales Basin since deposition ended at 10 Ma. More importantly, it implies the presence of topography ≥ 2 km in the core of the Aconcagua region of the Andes in the early Miocene, which is in stark contrast to that of the paleoelevation estimates from the Alto Tunuyán basin, despite similar positions within the mountain range.

5.4. Spatial pattern of surface uplift

Taken together, our data reveals a major N–S transition in the magnitude of late Miocene or later surface uplift (Fig. 6b). The 9–5 Ma record of paleoelevations similar to present-day elevations for the Iglesia Basin suggests that earlier deformation of the western Precordillera (Jordan et al., 1993, 2001) brought the adjacent wedge-top basin to its present elevation sometime before 9 Ma. To the south, the Manantiales Basin shows 0.8 $\pm$ 0.4 km of surface uplift of the basin since 10 Ma. The Uspallata Basin has undergone ~0.8 km $\pm$ 0.4 km of surface uplift since the late Miocene independent of the undated sediments south of the Río Mendoza. Farther south, the Alto Tunuyán basin must have experienced 2 km $\pm$ 0.5 km of surface uplift since the deposition of the Bútalo Formation. This pattern of Mio-Pliocene surface uplift is the exact opposite of the total crustal shortening and crustal thickness (Fig. 2C). There are several potential explanations for the spatial and temporal pattern in surface uplift.

5.4.1. Crustal shortening

North of 33°S the southward increase in post 10 Ma uplift may indeed reflect the N–S gradient in the onset of deformation of the Precordillera, which initiated in the early Miocene at ~30°S (Jordan et al., 1993; Ramos et al., 2002; Vergés et al., 2001; Walcek and Hoke, 2012). However, the total amounts of crustal shortening and crustal thickness (Fig. 2C) also decline dramatically south of 32°S despite similar amounts of observed surface uplift at Uspallata and Manantiales. South of 33°S, deformation of the Frontal and Principal cordilleras is recorded in middle and late Miocene synorogenic deposits, but the total crustal shortening achieved since the latest Miocene is insufficient to generate the observed 2 km of relief during the late Miocene to early Pliocene (Giambiagi et al., 2003, 2012; Fig. 2). There are no formal

estimates of the uncertainty on any of the shortening estimates (Allmendinger and Judge, 2013) complied here; however, we take the difference between the shortening estimates by Cristallini and Ramos (2000) and Allmendinger et al. (1990), ~15%, to reflect the real uncertainty in shortening estimates. At a more conservative 20% uncertainty, there remains a substantial N–S gradient in crustal shortening. Thus, we conclude that crustal shortening cannot completely explain the observed surface uplift pattern.

5.4.2. Influence of plate interactions

Temporal and spatial variations in the subduction angle of the Nazca plate have long been invoked to explain tectonic features of the Andes (e.g., Gutscher, 2002; Isacks, 1988; Jordan et al., 1983; Kay et al., 2005). Similarly, tectonic erosion of the leading edge of western South America (e.g., von Huene et al., 2004; e.g., von Huene and Scholl, 1991) has been proposed to explain sudden shifts in the location of the volcanic arc (Kay et al., 2005). At first glance there is a strong spatial correspondence between the surface uplift pattern (Fig. 6B) and the transition between the flat and steep slabs. Based on geochronologic and geochemical data from volcanic rocks, Kay et al. (2006) suggest a transient Miocene flat-slab episode from 8 to 5 Ma between 36°S and 38°S, with a rapid transition to steep subduction. Geometrically, this would induce a cirque shaped bowl in the geometry of the Nazca plate between 36°S and 33°S during the flat slab event. In a modeling study of the Cretaceous to present dynamic topography of the Colorado Plateau, the effect of the Farallon flat slab induced subsidence, followed by ~ 500 m of surface uplift (Liu and Gurnis, 2010). Even if this amount of uplift occurred over the steepening slab between 36°S and 38°S, as documented by Kay et al. (2006), only a fraction of that uplift signal would be transmitted 200 km north to the area of the Alto Tunuyán Basin at ~33.7°S.

5.4.3. Migration of a crustal root

In the absence of a strong correlation between the timing and magnitude of crustal shortening to the pattern of topographic change in the Andes, other potential influences must be explored. Farías et al. (2008) mapped contiguous, regionally extensive paleosurfaces in the Chilean Andes immediately adjacent to the Alto Tunuyán. Based on geochronology and numerical modeling of knickpoint retreat, these authors were able to estimate a late Miocene/early Pliocene initiation of surface uplift, with a total magnitude of ~2 km. Remarkably, our data for a low-elevation Alto Tunuyán Basin in the late Miocene corroborate their proposed timing and magnitude for surface uplift observed in Chile. Hoke et al. (2014a) also report evidence for low exhumation and high surface uplift in the Frontal Cordillera between 33°S and 33.75°S based on (U–Th)/He thermochronological data obtained from vertical profiles from the Río Mendoza and Río Tunuyán valleys. In addition, Giambiagi et al. (2014) propose a kinematic model based on a compilation of structural and geophysical data across the Andes where deformation migrates eastward once crustal thickness reaches 50 km. As part of this model, surface uplift occurs as the crustal root also migrates eastward in concert with ductile deformation of the lower crust. It is important to note that ductile deformation and root growth occurs west of the active thrust front under the core of the range (Fig. 7B; Giambiagi et al., 2014). At 34°S, this model reconciles the observed timing of deformation as well as the sequence and magnitudes of surface uplift from Farías et al. (2008) and is independent of a lithospheric mantle delamination mechanism or a transient slab-flattening episode, as proposed by Kay et al. (2005, 2006). The synchroneity across the range suggests rapid growth and largely eastward expansion of the crustal root during the Pliocene (Fig. 7B). The northward decrease in late Miocene to early Pliocene surface uplift suggests the crustal root achieved the critical 50 km thickness before that period and
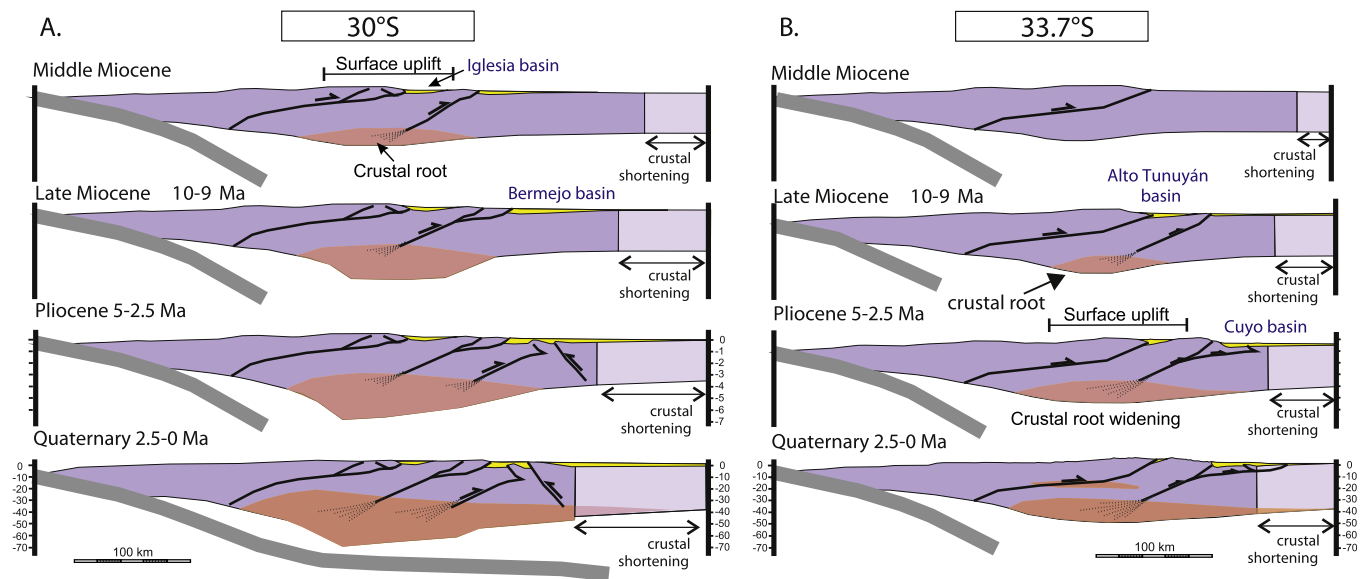
Fig. 7. A. Sequence of schematic, crustal-scale cross sections at 30°S. Note the that most of the shortening occurs in the Precordillera, thus much of the root expansion related to the elevation of the Iglesia Basin occurs prior to 9 Ma. B. Sequence of balanced, crustal-scale cross sections at 33.7°S adapted from Giambiagi et al. (2014) illustrating the growth, and rapid expansion of the crustal root which drives passive surface uplift of the Alto Tunuyan basin since the latest Miocene.

may be related to the N–S diachroneity of deformation in the Precordillera (Fig. 7A).

5.5. The growth of topography in narrow mountain ranges

Debates surrounding the evolution of mountains and continental plateaus have revolved around the relative role of crustal shortening, ductile crustal mass redistribution and erosion within the crust versus other lithospheric scale processes, such as delamination, in creating topography (e.g. Clark and Royden, 2000; DeCelles et al., 2009; Ehlers and Poulsen, 2009; Garzione et al., 2008; Hilley et al., 2004; Husson and Sempere, 2003; Montgomery et al., 2001). The Coulomb wedges typical of narrow mountain ranges should be simple systems and at first glance their topographic evolution should be tightly coupled in time and magnitude to crustal thickening. Yet, our data from the narrow portion of the Central Andes highlight that the topographic growth of a mountain range can be either tightly linked or entirely decoupled from crustal shortening and that crustal root formation via ductile deformation in the lower crust may result in passive surface uplift separated from brittle upper crustal deformation. In a mountain range with low exhumation rates, elevations should directly track the increase in crustal thickness, whereas high exhumation rates should maintain relatively constant topographies provided that erosion can keep pace with rock uplift and minimize increases in crustal thickness (e.g., England and Molnar, 1990). Based on the N–S gradients in accumulation (<2 km total thickness in the south compared with 4–12 km in the Bermejo Foreland of the north, Dávila and Carter, 2013) and the constant topography of the Iglesia wedge-top basin since 9 Ma, it would appear that exhumation is more efficient in the northern area and less efficient in the south. Thus, perhaps the topography of the range is more stable and less likely to change near 30°S where exhumation appears to be greater. Similarly, consistent with low exhumation on the eastern flanks of the range between 33°S and 35°S, the magnitude of surface uplift was greater as the crustal root expanded eastward (Fig. 7). Thus, our paleoaltimetry data highlight the interplay between surface uplift and exhumation in the topographic evolution of mountain ranges. However, given crustal thicknesses in the northern portion of our study area between 30 and 32°S (Gans et al., 2011; Figs. 2 and 7A), elevations should be much higher,

suggesting that the range and its immediately adjacent areas are held down by its root and/or the flat-slab and will experience considerable surface uplift when the flat slab transitions to a normal subduction geometry and lithospheric root is allowed to founder. The combined topographic response to slab steepening and lithospheric floundering of the crustal root would result in at least 2 km of surface uplift (e.g. Hoke and Garzione, 2008). Based on the spatial extent of crust >60 km thick in this region, an eastward expansion of high topography would extend into the western Sierras Pampeanas creating a broad high Plateau (Fig. 7A).

6. Conclusions

We used the $\delta^{18}O$ values of pedogenic carbonate from foreland and intermontane basin sediments preserved in different tectonic positions in the southern Central Andes of central Argentina. By designing our sampling to include sites that have always been east of the modern range front, we are able to control for regional variations in non-elevation related factors such as climate or environmental change. No major, coherent isotopic shifts $> 1\permil$ are observed in our isotope records, which span up to 10 Ma of the Miocene. Calculated elevations from samples east of the range front suggest these areas have been at or near their present elevation since the middle Miocene. While we do not capture topographic change in the isotopic records, there are significant differences between calculated elevations and modern elevations, which suggest surface uplift occurred over much of the area since the latest Miocene. Intermontane basins show a pronounced N–S gradient in surface uplift from 0 at the Iglesia Basin (30°S) to 2 km $\pm$ 0.5 km in the Alto Tunuyán Basin (34.7°S). This large gradient in surface uplift follows a pattern that is opposite to that of crustal thickness and total Neogene crustal shortening, suggesting that surface uplift is neither temporally nor spatially linked to crustal shortening. We ascribe the large magnitude surface uplift of the southern area to the time transient eastern migration of the crustal root as it attained a critical thickness of 50 km as described by Giambiagi et al. (2014).

Acknowledgements

Appendix A. Supplementary material

Supplementary material related to this article can be found online at http://dx.doi.org/10.1016/j.epsl.2014.08.032.

References

Allmendinger, R.W., Judge, P., 2013. Stratigraphic uncertainty and errors in shortening from balanced sections in the North American Cordillera. Geol. Soc. Am. Bull. 125, 1569–1579. http://dx.doi.org/10.1130/B30871.1.

Allmendinger, R.W., Figueroa, D., Snyder, D., Beer, J., Mpodozis, C., Isacks, B.L., 1990. Foreland shortening and crustal balancing in the Andes at 30-degrees-S latitude. Tectonics 9, 789–809. http://dx.doi.org/10.1029/TC009i004p00789.

Anderson, M., Alvarado, P., Zandt, G., Beck, S., 2007. Geometry and brittle deformation of the subducting Nazca Plate, Central Chile and Argentina. Geophys. J. Int. 171, 419–434. http://dx.doi.org/10.1111/j.1365-246X.2007.03483.x.

Beer, J.A., Allmendinger, R.W., Figueroa, D.E., Jordan, T.E., 1990. Seismic stratigraphy of a Neogene piggyback basin, Argentina. Am. Assoc. Pet. Geol. Bull. 74, 1183–1202.

Blisniuk, P.M., Stern, L.A., 2005. Stable isotope paleoaltimetry: a critical review. Am. J. Sci. 305, 1033–1074. http://dx.doi.org/10.2475/ajs.305.10.1033.

Bookhagen, B., Strecker, M.R., 2008. Orographic barriers, high-resolution TRMM rainfall, and relief variations along the eastern Andes. Geophys. Res. Lett. 35, L06403. http://dx.doi.org/10.1029/2007GL032011.

Cahill, T., Isacks, B.L., 1992. Seismicity and shape of the subducted Nazca Plate. J. Geophys. Res., Solid Earth 97, 17503–17529. http://dx.doi.org/10.1029/92JB00493.

Cerling, T.E., Quade, J., 1993. Stable carbon and oxygen isotopes in soil carbonates. In: Swart, P.K., Lohmann, K.C., McKenzie, J., Savin, S.M. (Eds.), Climate Change in Continental Isotopic Records. American Geophysical Union, Washington, DC, pp. 217–231. http://dx.doi.org/10.1029/GM078p0217.

Chamberlain, C.P., Poage, M.A., Craw, D., Reynolds, R.C., 1999. Topographic development of the Southern Alps recorded by the isotopic composition of authigenic clay minerals, South Island, New Zealand. Chem. Geol. 155, 279–294. http://dx.doi.org/10.1016/S0009-2541(98)00165-X.

Clark, M.K., Royden, L.H., 2000. Topographic ooze: building the eastern margin of Tibet by lower crustal flow. Geology 28, 703–706. http://dx.doi.org/10.1130/0091-7613(2000)28<703:TOBTEM>2.0.CO;2.

Cortés, J.M., 1993. El frente de corrimiento de la Cordillera Frontal y el extremo sur del valle de Uspallata, Mendoza. In: Ramos, V. (Ed.), XII° Congreso Geológico Argentino y II Congreso de Exploración de Hidrocarbouros, Buenos Aires, pp. 168–178.

Cristallini, E.O., Ramos, V.A., 2000. Thick-skinned and thin-skinned thrusting in the La Ramada fold and thrust belt: crustal evolution of the High Andes of San Juan, Argentina (32°SL). Tectonophysics 317, 205–235. http://dx.doi.org/10.1016/S0040-1951(99)00276-0.

Dávila, F.M., Carter, A., 2013. Exhumation history of the Andean broken foreland revisited. Geology 41, 443–446. http://dx.doi.org/10.1130/G33960.1.

DeCelles, P.G., Giles, K.A., 1996. Foreland basin systems. Basin Res. 8, 105–123. http://dx.doi.org/10.1046/j.1365-2117.1996.01491.x.

DeCelles, P., Ducea, M., Kapp, P., Zandt, G., 2009. Cyclicity in Cordilleran orogenic systems. Nat. Geosci. 2, 251–257. http://dx.doi.org/10.1038/ngeo469.

Ehlers, T.A., Poulsen, C.J., 2009. Influence of Andean uplift on climate and paleoaltimetry estimates. Earth Planet. Sci. Lett. 281, 238–248. http://dx.doi.org/10.1016/j.epsl.2009.02.026.

Eiler, J.M., 2007. "Clumped-isotope" geochemistry—the study of naturally-occurring, multiply-substituted isotopologues. Earth Planet. Sci. Lett. 262, 309–327. http://dx.doi.org/10.1016/j.epsl.2007.08.020.

England, P., Molnar, P., 1990. Surface uplift, uplift of rocks, and exhumation of rocks. Geology 18, 1173–1177. http://dx.doi.org/10.1130/0091-7613(1990)018<1173:SUUORA>2.3.CO;2.

Farías, M., Charrier, R., Carretier, S., Martinod, J., Fock, A., Campbell, D., Cáceres, J., Comte, D., 2008. Late Miocene high and rapid surface uplift and its erosional response in the Andes of Central Chile (33°–35°S). Tectonics 27, TC1005. http://dx.doi.org/10.1029/2006TC002046.

Gans, C.R., Beck, S.L., Zandt, G., Gilbert, H., Alvarado, P., Anderson, M., Linkimer, L., 2011. Continental and oceanic crustal structure of the Pampean flat slab region, western Argentina, using receiver function analysis: new high-resolution results. Geophys. J. Int. 186, 45–58. http://dx.doi.org/10.1111/j.1365-246X.2011.05023.x.

García, V.H., Casa, A.L., 2014. Quaternary tectonics and seismic potential of the Andean retrowedge at 33–34°S. In: Sepulveda, S.A., Giambiagi, L.B., Moreiras, S.M., Pinto, L., Tunik, M.A., Hoke, G.D., Farías, M. (Eds.), Geodynamic Processes in the Andes of Central Chile and Argentina. In: Geological Society (London) Special Publications, London. http://dx.doi.org/10.1144/SP399.11.

Garreaud, R.D., Vuille, M., Compagnucci, R., Marengo, J., 2009. Present-day South American climate. Palaeogeogr. Palaeoclimatol. Palaeoecol. 281, 180–195. http://dx.doi.org/10.1016/j.palaeo.2007.10.032.

Garzione, C.N., Dettman, D.L., Quade, J., DeCelles, P.G., Butler, R.F., 2000. High times on the Tibetan Plateau: paleoelevation of the Thakkhola graben, Nepal. Geology 28, 339–342. http://dx.doi.org/10.1130/0091-7613(2000)28<339:HTOTTP>2.0.CO;2.

Garzione, C.N., Hoke, G.D., Labarkin, J.C., Withers, S., MacFadden, B.J., Ghosh, P., Mulch, A., 2008. Rise of the Andes. Science 320, 1304–1307. http://dx.doi.org/10.1126/science.1148615.

Gehrels, G.E., Valencia, V.A., Ruiz, J., 2008. Enhanced precision, accuracy, efficiency, and spatial resolution of U–Pb ages by laser ablation-multicollector-inductively coupled plasma-mass spectrometry. Geochem. Geophys. Geosyst. 9. http://dx.doi.org/10.1029/2007GC001805.

Giambiagi, L.B., 1999. Los depositos Neogenos de la region del Rio Palomares, Cordillera Principal de Mendoza. Rev. Asoc. Geol. Argent. 54, 47–59.

Giambiagi, L.B., Tunik, M.A., Ghiglione, M., 2001. Cenozoic tectonic evolutino of the Alto Tunuyán foreland basin above the transition zone between the flat and normal subduction segment (33°30′–34°S), western Argentina. J. South Am. Earth Sci. 14, 707–724. http://dx.doi.org/10.1016/S0895-9811(01)00059-1.

Giambiagi, L.B., Ramos, V.A., Godoy, E., Alvarez, P.P., Orts, S., 2003. Cenozoic deformation and tectonic style of the Andes, between 33 degrees and 34 degrees south latitude. Tectonics 22, 1041. http://dx.doi.org/10.1029/2001TC001354.

Giambiagi, L.B., Mescua, J., Bechis, F., Martinez, A., Folguera, A., 2011. Pre-Andean deformation of the Precordillera southern sector, southern Central Andes. Geosphere 7, 219–239. http://dx.doi.org/10.1130/GES00572.1.

Giambiagi, L.B., Mescua, J., Bechis, F., Tassara, A., Hoke, G., 2012. Thrust belts of the southern Central Andes: along-strike variations in shortening, topography, crustal geometry, and denudation. Geol. Soc. Am. Bull. 124, 1339–1351. http://dx.doi.org/10.1130/B30609.1.

Giambiagi, L., Tassara, A., Mescua, J., Tunik, M.A., Alvarez, P., Godoy, E., Hoke, G., Pinto, L., Spagnotto, S., Porras, H., Tapia, P.M., Jara, P., Bechis, F., Garcia, V., Suriano, J., Paganoni, S., 2014. Evolution of shallow and deep structures along the Maipo–Tunuyán Transect (33°40′S). In: Supelveda, S., Giambiagi, L., Moreiras, S., Pinto, L., Tunik, M.A., Hoke, G., Farias, M. (Eds.), Geodynamic Processes in the Andes of central Chile and Argentina. Geological Society of London, London. http://dx.doi.org/10.1144/SP399.14.

Gutscher, M., 2002. Andean subduction styles and their effect on thermal structure and interplate coupling. J. South Am. Earth Sci. 15, 3–10. http://dx.doi.org/10.1016/S0895-9811(02)00002-0.

Haselton, K., Hilley, G., Strecker, M.R., 2002. Average Pleistocene climatic patterns in the southern Central Andes: controls on mountain glaciation and paleoclimate implications. J. Geol. 110, 211–226. http://dx.doi.org/10.1086/338414.

Hilley, G.E., Strecker, M.R., Ramos, V.A., 2004. Growth and erosion of fold-and-thrust belts with an application to the Aconcagua fold-and-thrust belt. J. Geophys. Res., Solid Earth 109. http://dx.doi.org/10.1029/2002JB002282.

Hoke, G.D., Garzione, C.N., 2008. Paleosurfaces, paleoelevation, and the mechanisms for the latest Miocene topographic development of the Altiplano Plateau. Earth Planet. Sci. Lett. 271, 192–201. http://dx.doi.org/10.1016/j.epsl.2008.04.008.

Hoke, G.D., Garzione, C.N., Araneo, D.C., Latorre, C., Strecker, M.R., Williams, K.J., 2009. The stable isotope altimeter: do Quaternary pedogenic carbonates predict modern elevations? Geology 34.

Hoke, G.D., Aranibar, J.N., Viale, M., Araneo, D.C., Llano, C., 2013. Seasonal moisture sources and the isotopic composition of precipitation, rivers and carbonates across the Andes at 32.5–35.5°S. Geochem. Geophys. Geosyst. 14, 962–978. http://dx.doi.org/10.1002/ggge.20045.

Hoke, G.D., Graber, N.R., Mescua, J., Giambiagi, L., Fitzgerald, P., Metcalf, J., 2014a. Near pure surface uplift of the Argentine Frontal Cordillera: insights from (U–Th)/He thermochronometry and geomorphic analysis. In: Supelveda, S., Giambiagi, L., Moreiras, S., Pinto, L., Tunik, M.A., Hoke, G., Farias, M. (Eds.), Geodynamic Processes in the Andes of Central Chile and Argentina. Geological Society of London, London. http://dx.doi.org/10.1144/SP399.4.

Hoke, G.D., Liu-Zeng, J., Hren, M.T., Wissink, G.K., Garzione, C.N., 2014b. Stable isotopes reveal high southeast Tibetan Plateau margin since the Paleogene. Earth Planet. Sci. Lett. 394, 270–278. http://dx.doi.org/10.1016/j.epsl.2014.03.007.

Hren, M.T., Pagani, M., Erwin, D.M., Brandon, M., 2010. Biomarker reconstruction of the early Eocene paleotopography and paleoclimate of the northern Sierra Nevada. Geology 38, 7–10. http://dx.doi.org/10.1130/G30215.1.

Husson, L., Sempere, T., 2003. Thickening the Altiplano crust by gravity-driven crustal channel flow. Geophys. Res. Lett. 30, 1243. http://dx.doi.org/10.1029/2002GL016877.

Hynek, S.A., Passey, B.H., Prado, J.L., Brown, F.H., Cerling, T.E., Quade, J., 2012. Small mammal carbon isotope ecology across the Miocene–Pliocene boundary, northwestern Argentina. Earth Planet. Sci. Lett. 321–322, 177–188. http://dx.doi.org/10.1016/j.epsl.2011.12.038.

Insel, N., Poulsen, C.J., Sturm, C., Ehlers, T.A., 2013. Climate controls on Andean precipitation δ^{18}O interannual variability. J. Geophys. Res., Atmos. 118, 1–22. http://dx.doi.org/10.1002/jgrd.50619.

Irigoyen, M.V., Buchan, K.L., Brown, R.L., 2000. Magnetostratigraphy of Neogene Andean foreland-basin strata, lat 33°S, Mendoza Province, Argentina. Geol. Soc. Am. Bull. 112, 803–816. http://dx.doi.org/10.1130/0016-7606(2000)112<803:MONAFS>2.0.CO;2.

Isacks, B.L., 1988. Uplift of the Central Andean Plateau and bending of the Bolivian Orocline. J. Geophys. Res. 93, 3211–3231. http://dx.doi.org/10.1029/JB093iB04p03211.

Jeffery, M., Poulsen, C., Ehlers, T.A., 2012. Impacts of Cenozoic global cooling, surface uplift, and an inland seaway on South American paleoclimate and precipitation δ18O. Geol. Soc. Am. Bull. 124, 1027–1047. http://dx.doi.org/10.1130/B30480.1.

Jordan, T., Isacks, B.L., Allmendinger, R.W., Brewer, J.A., Ramos, V.A., Ando, C.J., 1983. Andean tectonics related to geometry of subducted Nazca Plate. Geol. Soc. Am. Bull. 94, 341–361. http://dx.doi.org/10.1130/0016-7606(1983)94<341:ATRTGO>2.0.CO;2.

Jordan, T., Allmendinger, R.W., Damanti, J.F., Drake, R.E., 1993. Chronology of motion in a complete thrust belt – the Precordillera, 30–31-degrees-S, Andes Mountains. J. Geol. 101, 135–156.

Jordan, T., Tamm, V., Figueroa, G., Flemings, P.B., Richards, D., Tabbutt, K., Cheatham, T., 1996. Development of the Miocene Manantiales foreland basin, Principal Cordillera, San Juan, Argentina. Rev. Geol. Chile 23, 43–79.

Jordan, T., Schlunegger, F., Cardozo, N., 2001. Unsteady and spatially variable evolution of the Neogene Andean Bermejo foreland basin, Argentina. J. South Am. Earth Sci. 14, 775–798. http://dx.doi.org/10.1016/S0895-9811(01)00072-4.

Kay, S.M., Mpodozis, C., 2002. Magmatism as a probe to the Neogene shallowing of the Nazca plate beneath the modern Chilean flat-slab. J. South Am. Earth Sci. 15, 39–57. http://dx.doi.org/10.1016/S0895-9811(02)00005-6.

Kay, S.M., Maksaev, V., Moscoso, R., Mpodozis, C., Nasi, C., 1987. Probing the evolving Andean lithosphere – mid-late Tertiary magmatism in Chile (29-degrees–30-degrees–30'S) over the modern zone of subhorizontal subduction. J. Geophys. Res., Solid Earth 92, 6173–6189. http://dx.doi.org/10.1029/JB092iB07p06173.

Kay, S.M., Godoy, E., Kurtz, A., 2005. Episodic arc migration, crustal thickening, subduction erosion, and magmatism in the south-Central Andes. Geol. Soc. Am. Bull. 117, 67–88. http://dx.doi.org/10.1130/B25431.1.

Kay, S., Burns, M., Copeland, P., Ramos, V., 2006. Upper Cretaceous to Holocene magmatism and evidence for transient Miocene shallowing of the Andean subduction zone under the northern Neuquén Basin. In: Ramos, V., Kay, S. (Eds.), Evolution of an Andean Margin: A Tectonic and Magmatic View from the Andes to the Neuquén Basin (35°–39°S Lat). Geological Society of America, Boulder, CO, pp. 19–60. http://dx.doi.org/10.1130/2006.2407(02).

Kim, S.-T., O'Neil, J.R., 1997. Equilibrium and nonequilibrium oxygen isotope effects in synthetic carbonates. Geochim. Cosmochim. Acta 61, 3461–3475. http://dx.doi.org/10.1016/S0016-7037(97)00169-5.

Klappa, C.F., 1980. Rhizoliths in terrestrial carbonates: classification, recognition, genesis and significance. Sedimentology 27, 613–629. http://dx.doi.org/10.1111/j.1365-3091.1980.tb01651.x.

Lamb, S., 2011. Did shortening in thick crust cause rapid Late Cenozoic uplift in the northern Bolivian Andes? J. Geol. Soc. 168, 1079–1092. http://dx.doi.org/10.1144/0016-76492011-008.

Latorre, C., Quade, J., McIntosh, W., 1997. The expansion of C-4 grasses and global change in the late Miocene: stable isotope evidence from the Americas. Earth Planet. Sci. Lett. 146, 83–96. http://dx.doi.org/10.1016/S0012-821X(96)00231-2.

Leier, A., Quade, J., DeCelles, P., Kapp, P., 2009. Stable isotopic results from paleosol carbonate in South Asia: paleoenvironmental reconstructions and selective alteration. Earth Planet. Sci. Lett. 279, 242–254. http://dx.doi.org/10.1016/j.epsl.2008.12.044.

Liu, L., Gurnis, M., 2010. Dynamic subsidence and uplift of the Colorado Plateau. Geology 38, 663–666. http://dx.doi.org/10.1130/G30624.1.

Meade, B.J., Conrad, C.P., 2008. Andean growth and the deceleration of South American subduction: time evolution of a coupled orogen-subduction system. Earth Planet. Sci. Lett. 275, 93–101. http://dx.doi.org/10.1016/j.epsl.2008.08.007.

Mirré, J.C., 1966. Geología del Valle del Río de los Patos (entre Barreal y Las Hornillas). Revista de la Asociacion Geologica Argentina 21, 211–231.

Mix, H.T., Mulch, A., Kent-Corson, M.L., Chamberlain, C.P., 2011. Cenozoic migration of topography in the North American Cordillera. Geology 39, 87–90. http://dx.doi.org/10.1130/G31450.1.

Montgomery, D.R., Balco, G., Willett, S.D., 2001. Climate, tectonics, and the morphology of the Andes. Geology 29, 579–582. http://dx.doi.org/10.1130/0091-7613(2001)029<0579:CTATMO>2.0.CO;2.

Mpodozis, C., Ramos, V., 1989. The Andes of Chile and Argentina. In: Ericksen, G.E., Cañas Pinochet, M.T., Reinemund, J.A. (Eds.), Geology of the Andes and Its Relation to Hydrocarbon and Mineral Resources. Circum-Pacific Council for Energy and Mineral Resources, Houston, Texas, pp. 56–90.

Mulch, A., Graham, S.A., Chamberlain, C.P., 2006. Hydrogen isotopes in Eocene river gravels and paleoelevation of the Sierra Nevada. Science 313, 87–89. http://dx.doi.org/10.1126/science.1125986.

Peters, N.A., Huntington, K.W., Hoke, G.D., 2013. Hot or not? Impact of seasonally variable soil carbonate formation on paleotemperature and O-isotope records from clumped isotope thermometry. Earth Planet. Sci. Lett. 361, 208–218. http://dx.doi.org/10.1016/j.epsl.2012.10.024.

Poage, M., Chamberlain, C., 2001. Empirical relationships between elevation and the stable isotope composition of precipitation and surface waters: considerations for studies of paleoelevation change. Am J. Sci. 301, 1–15.

Ramos, V.A., Cristallini, E., Pérez, D.J., 2002. The Pampean flat-slab of the Central Andes. J. South Am. Earth Sci. 15, 59–78. http://dx.doi.org/10.1016/S0895-9811(02)00006-8.

Rowley, D., 2007. Stable isotope-based paleoaltimetry: theory and validation. Rev. Mineral. Geochem. 66, 23–52. http://dx.doi.org/10.2138/rmg.2007.66.2.

Rowley, D.B., Currie, B.S., 2006. Paleo-altimetry of the late Eocene to Miocene Lunpola basin, central Tibet. Nature 439, 677–681. http://dx.doi.org/10.1038/nature04506.

Rowley, D.B., Garzione, C.N., 2007. Stable isotope-based paleoaltimetry. Annu. Rev. Earth Planet. Sci. 35, 463–508. http://dx.doi.org/10.1146/annurev.earth.35.031306.140155.

Ruskin, B.G., Jordan, T.E., 2007. Climate change across continental sequence boundaries: paleopedology and lithofacies of Iglesia Basin, Northwestern Argentina. J. Sediment. Res. 77, 661–679. http://dx.doi.org/10.2110/jsr.2007.069.

Sruoga, P., Etcheverría, M., Folgera, A., Repol, D., Zanettini, J.C., 2005. Hoja geoloica 3569-I, Volcán Maipo. Programa Nacional de Cartas Geológicas de la República Argentina. Servicio Geologico Minero Argentino, Buenos Aires.

Strecker, M.R., Alonso, R.N., Bookhagen, B., Carrapa, B., Hilley, G.E., Sobel, E.R., Trauth, M.H., 2007. Tectonics and climate of the Southern Central Andes. Annu. Rev. Earth Planet. Sci. 35, 747–787. http://dx.doi.org/10.1146/annurev.earth.35.031306.140158.

Sturm, C., Hoffmann, G., Langmann, B., 2007. Simulation of the stable water isotopes in precipitation over South America: comparing regional to global circulation models. J. Climate 20, 3730–3750. http://dx.doi.org/10.1175/JCLI4194.1.

Thomas, W.A., Astini, R.A., 1996. The Argentine Precordillera: a traveler from the Ouachita embayment of North American Laurentia. Science 273, 752–757. http://dx.doi.org/10.1126/science.273.5276.752.

Vergés, J., Ramos, E., Seward, D., Busquets, P., Colombo, F., 2001. Miocene sedimentary tectonic evolution of the Andean Precordillera at 31°S, Argentina. J. South Am. Earth Sci. 14, 735–750. http://dx.doi.org/10.1016/S0895-9811(01)00070-0.

Vicente, J.C., 2005. La fase primordial de estructuracion de la faja plegada y corrida del Aconcagua; importancia de la fase Pehuenche del Mioceno inferior. Revista de la Asociacion Geologica Argentina 60, 672–684.

von Gosen, W., 1992. Structural evolution of the Argentine Precordillera — the Rio–San–Juan section. J. Struct. Geol. 14, 643–667. http://dx.doi.org/10.1016/0191-8141(92)90124-F.

von Huene, R., Scholl, D.W., 1991. Observations at convergent margins concerning sediment subduction, subduction erosion, and the growth of continental-crust. Rev. Geophys. 29, 279–316. http://dx.doi.org/10.1029/91RG00969.

von Huene, R., Ranero, C.R., Vannuchhi, P., 2004. Generic model of subduction erosion. Geology 32, 913–916. http://dx.doi.org/10.1130/G20563.1.

Walcek, A., Hoke, G., 2012. Surface uplift and erosion of the southernmost Argentine Precordillera. Geomorphology 153–154, 156–168. http://dx.doi.org/10.1016/j.geomorph.2012.02.021.

Whipple, K.X., Meade, B.J., 2006. Orogen response to changes in climatic and tectonic forcing. Earth Planet. Sci. Lett. 243, 218–228. http://dx.doi.org/10.1016/j.epsl.2005.12.022.

Willett, S.D., 1999. Orogeny and orography; the effects of erosion on the structure of mountain belts. J. Geophys. Res. 104, 28,957–928,982. http://dx.doi.org/10.1029/1999JB900248.